

Study of the ^{133}Ba nucleus with the (\vec{d}, p) reaction

G. Suliman^{1,a}, D. Bucurescu^{1,2}, C. Rusu³, R. Hertzenberger⁴, H.-F. Wirth⁴, T. Faestermann⁵, R. Krücken⁵, K. Wimmer⁵, T. Behrens⁵, V. Bildstein⁵, K. Eppinger⁵, C. Hinke⁵, M. Mahgoub⁵, P. Meierbeck⁵, M. Reithner⁵, S. Schwertel⁵, and N. Chauvin⁶

¹ Horia Hulubei National Institute of Physics and Nuclear Engineering (IFIN-HH), R-77125 Bucharest, Romania

² Academy of Romanian Scientists, 54 Splaiul Independenței, 050094 Bucharest, Romania

³ University of Texas at Dallas, School of Natural Sciences and Mathematics, Richardson, TX-75080, USA

⁴ Fakultät für Physik, Ludwig-Maximilians-Universität München, D-85748 Garching, Germany

⁵ Physik-Department, Technische Universität München, D-85748 Garching, Germany

⁶ Centre de Spectrométrie Nucléaire et Spectrométrie de Masse, CNRS/IN2P3, Université Paris-Sud, UMR8609, ORSAY-Campus, F-91405 France

Received: 26 March 2009 / Revised: 23 June 2009

Published online: 21 August 2009 – © Società Italiana di Fisica / Springer-Verlag 2009

Communicated by N. Alamanos

Abstract. Excited states in ^{133}Ba were studied with the $^{132}\text{Ba}(\vec{d}, p)^{133}\text{Ba}$ reaction at 24.0 MeV, with a polarized deuteron beam using the Munich magnetic spectrograph Q3D. Many unambiguous spin-parity assignments were made up to an excitation energy of 2.2 MeV, which allow a detailed comparison with different theoretical calculations, such as the interacting boson-fermion model and the shell model.

PACS. 21.10.-k Properties of nuclei; nuclear energy levels – 21.60.Ev Collective models – 25.40.Hs Transfer reactions – 27.60.+j $90 \leq A \leq 149$

1 Introduction

The barium isotopes with less than 80 neutrons belong to a region of structural changes generally associated with nuclei being soft in the γ -deformation degree of freedom. In the framework of the interacting boson model (IBM) [1], the γ -soft nuclei are close to the so-called $O(6)$ dynamical symmetry. The first assignment of $O(6)$ properties to the Ba nuclei was made by pointing out the similarity of the $A \approx 130$ isotopes with the well-established $O(6)$ region in the Pt nuclei [2]. A finer distinction became possible with the introduction of phase transitions between different dynamical symmetries. In particular, in this nuclear region, ^{134}Ba was found [3] to present to a large extent the features of the $E(5)$ symmetry [4], which represents a (second-order) phase transition between the vibrator ($U(5)$ dynamical limit) and the γ -soft rotor ($O(6)$).

Dynamical symmetries can also be formulated for the odd-mass nuclei, as mixed, bosonic and fermionic systems. Such an approach is especially interesting close to the critical-point transition in the even-even nuclei. Such a Bose-Fermi symmetry, named $E(5/4)$, was developed for odd-mass nuclei where a $j = 3/2$ particle is coupled to an $E(5)$ core [5]. The restriction of the fermionic space

to a single- j orbit is, however, a strong approximation, and therefore a more realistic case was considered, with a particle in the $j = 1/2, 3/2,$ and $5/2$ orbits coupled to an $E(5)$ core, this symmetry being called $E(5/12)$ [6]. Because of the complexity of the coupling between an odd particle and an even-even core, the study of criticality in odd-mass nuclei is very interesting, both as an application to specific nuclei, and for the study of the influence of the odd particle on the nuclear phase transition. On the other hand, the increased complexity of the odd-mass nuclei level schemes makes such studies experimentally more difficult.

In the region around the Ba isotopes there was only one attempt to test the predictions of the $E(5/4)$ symmetry, namely, in the ^{135}Ba nucleus [7], with the conclusion that this symmetry appears considerably more broken than the $E(5)$ one in the even-even core.

The current study of the ^{133}Ba nucleus has as purpose a more reliable determination of the structure of this neighbour of the critical-point nucleus ^{134}Ba , which could serve both to investigate the critical phase transition in odd-mass nuclei and to better evaluate different structure models in this region. Indeed, the known level scheme of ^{133}Ba [8] presents many ambiguous spin and parity assignments even for levels below 1.0 MeV. The present information on low-lying levels in this nucleus comes mainly

^a e-mail: suligab@tandem.nipne.ro

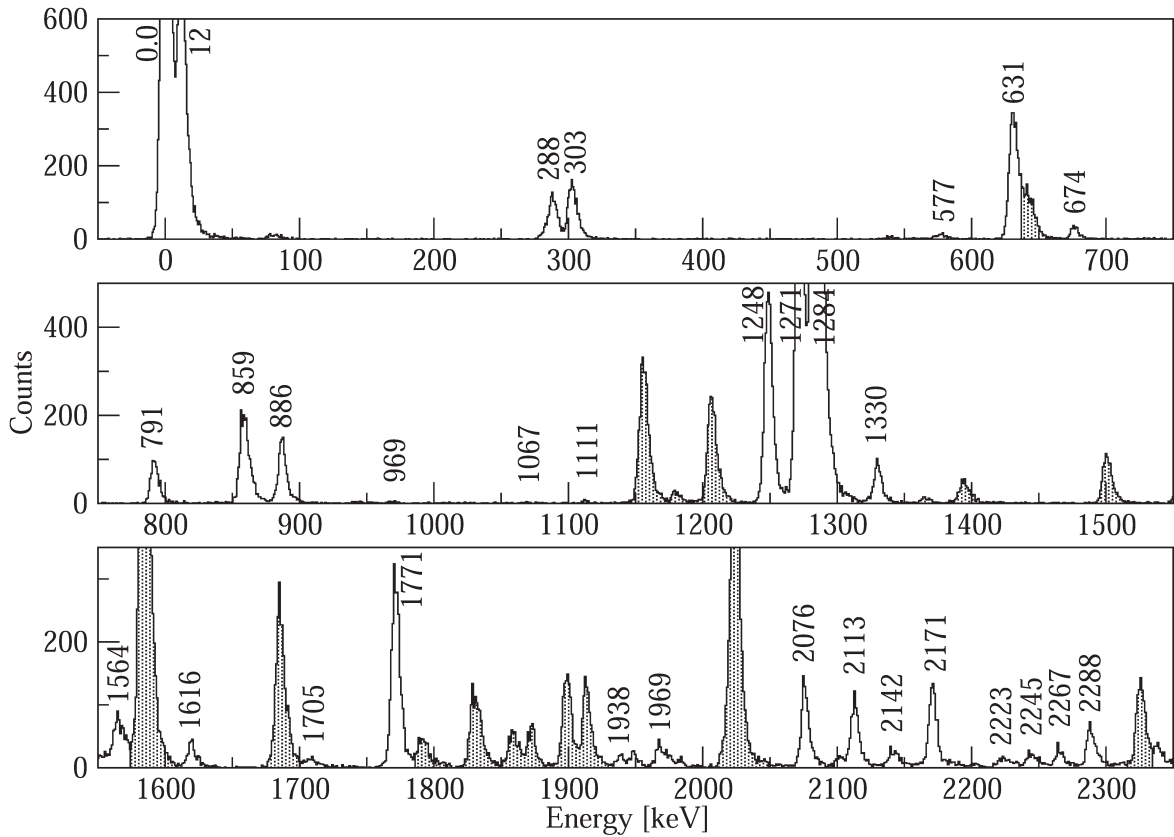


Fig. 1. Example of the spectrum of the $^{132}\text{Ba}(\vec{d}, p)$ reaction, for one of the beam spin orientation, measured at the angle of 6° ; the shaded peaks were identified as due to the chlorine impurities present in the target. The peaks are labeled with the excitation energy in ^{133}Ba .

from the β^+ decay of ^{133}La [9], the study of the decay of its isomeric $11/2^-$ state [10] (for earlier articles, see [8]), and one study of the (d, p) direct transfer reaction [11]. High-spin states were investigated via the $^{124}\text{Sn}(^{12}\text{C}, 3n\gamma)$ reaction [12].

In this work we present the results of a study based on the (\vec{d}, p) transfer reaction at 24 MeV incident energy. The good isotopic enrichment of the target, the excellent energy resolution of the Munich magnetic spectrograph, and the use of a polarized deuteron beam enabled many unambiguous J^π assignments for states up to 2.3 MeV excitation. The present level scheme of ^{133}Ba is then compared to different theoretical predictions, including shell model calculations.

2 Experiment

2.1 The measurements

The $^{132}\text{Ba}(\vec{d}, p)^{133}\text{Ba}$ experiment was performed with the polarized deuteron beam delivered by the Stern-Gerlach ion source [13] and accelerated to 24.0 MeV by the MP Tandem accelerator at the Maier-Leibnitz Laboratory of the LMU and TUM. The beam vector polarization was around 78%.

The target consisted of $60 \mu\text{g}/\text{cm}^2$ of ^{132}Ba implanted in a $40 \mu\text{g}/\text{cm}^2$ carbon foil, and it was produced at the SIDONIE isotope separator of CSNSM-Orsay [14] starting from BaCO_3 material enriched 11.9% in ^{132}Ba .

After passing through the target, the deuteron beam was collected in a Faraday cup and the integrated current was used to normalize the different runs. The typical beam current on the target was around 500 nA. The reaction products were analyzed with the Q3D spectrograph [15] and then detected in a 1 m long focal-plane detector with cathode strip readout [16, 17], which performed ΔE - E_{rest} particle identification and position determination. The acceptance of the spectrograph was set at 2.42 msr (horizontal $\pm 4 \text{ mm}$ and vertical $\pm 20 \text{ mm}$).

The emergent particles were measured at 10 different angles of the spectrograph, between 6° and 40° . At each angle, the measurements were made for two different magnetic settings of the spectrograph to cover excitation energies from 0 to about 2.4 MeV. In each case, two spectra were collected, corresponding to the two orientations (“up” and “down”) of the incident beam spin, thus giving a total of four spectra measured at each angle.

For the energy calibration of spectra, we used well-known levels in ^{133}Ba , as well as the $^{144}\text{Sm}(d, p)$ reaction, which was measured at 10° with the same magnetic settings as our spectrum, with a $49 \mu\text{g}/\text{cm}^2$ thick target on

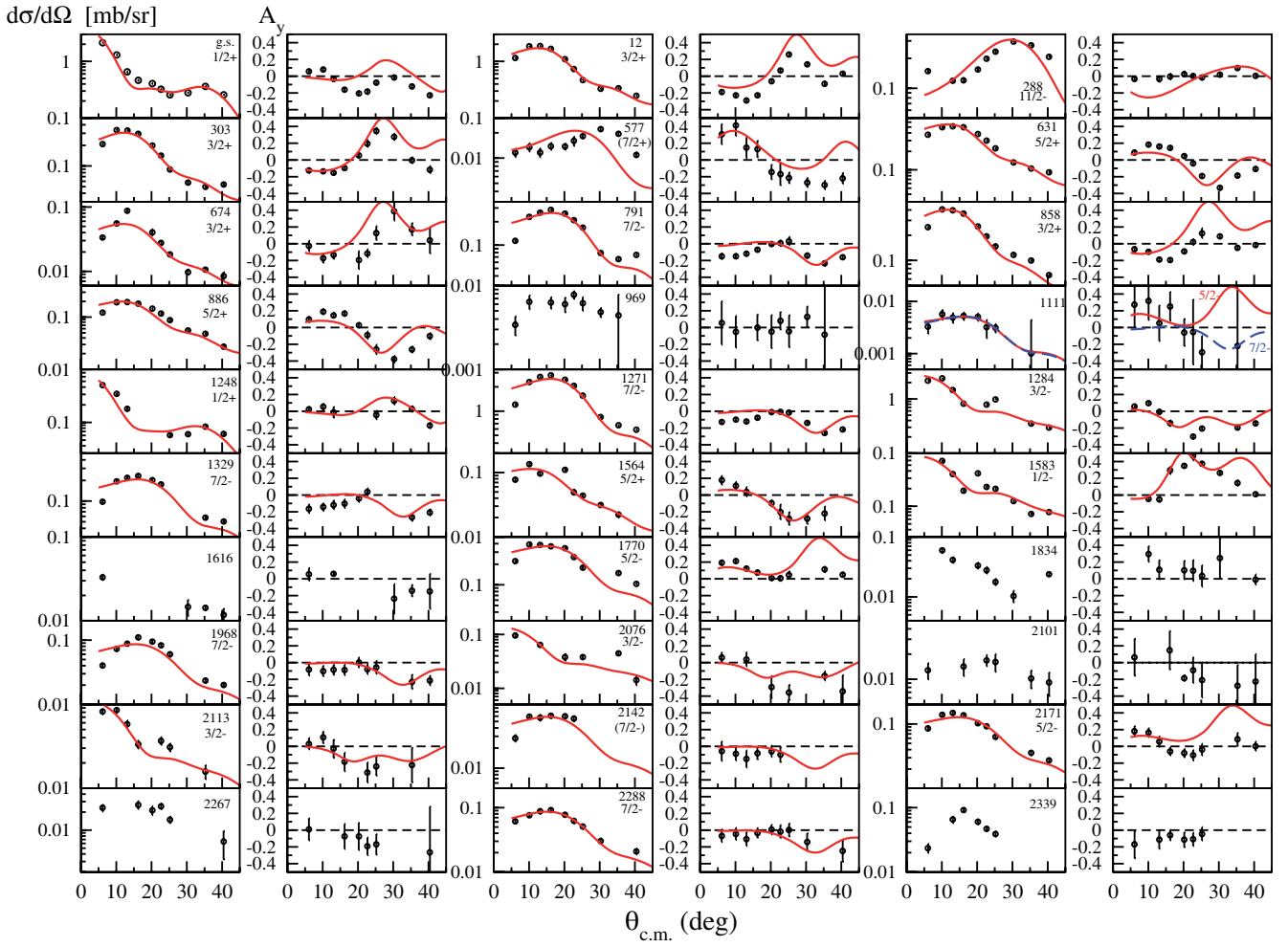


Fig. 2. Angular distributions and analyzing powers measured in the $^{132}\text{Ba}(\vec{d}, p)$ reaction for most of the levels listed in table 1. For each level, the left-side graph represents the cross-section angular distribution, while the right-side one (y -axis not labeled) the analyzing power, respectively. The continuous curves represent the DWBA calculated cross-sections (normalized to the data points), or the analyzing powers, respectively. The adopted spin values shown for most of the levels correspond to the information given by the analysis of the analyzing power.

$16 \mu\text{g}/\text{cm}^2$ carbon backing. This reaction provided very good calibration peaks up to 2.3 MeV excitation in our reaction [18].

2.2 DWBA analysis and results

Figure 1 shows the spectrum obtained at the laboratory angle of 6° , for the “up” orientation of the beam spin. The overall FWHM energy resolution was of 6–7 keV, being mostly determined by the target. While the spectra were practically background free, there was a contamination, especially troublesome in the higher excitation energy region, due to the (d, p) reaction on both stable isotopes of chlorine, ^{35}Cl and ^{37}Cl (^{37}Cl was also seen in another experiment, the (p, t) reaction, on the same target [19]). These contaminant peaks could be easily observed because of their different kinematics, but unfortunately they obscured many peaks of ^{133}Ba at certain angles.

The angular distributions and the analyzing powers obtained in the present experiment are shown in fig. 2. The differential cross-section at each angle of the angular distribution was obtained by averaging the cross-sections obtained for the two beam orientations, $d\sigma/d\Omega = \frac{\sigma_+ + \sigma_-}{2}$, and the analyzing power was determined using the relation $A_y = \frac{2}{3P_3} \frac{\sigma_+ - \sigma_-}{\sigma_+ + \sigma_-}$, where σ_+ , σ_- are the differential cross-sections measured for the two orientations of the beam spin, and P_3 is the vector polarisation of the beam.

Table 1 gives a summary of the levels observed: excitation energy, representative cross-section value, transferred orbital angular momentum, spin/parity assignment, and spectroscopic factor, in comparison with the ENSDF adopted levels [8] and with the previous (d, p) experiment [11]. The level energies provided by our measurements have an error generally smaller than 0.5 keV.

The orbital angular momentum transfer (l) and the spin (J) of each state have been assigned by comparing the measured data with calculations performed with the

Table 1. List of the levels observed in the present experiment, compared to the ENSDF adopted levels [8], and with those observed in the previous (d, p) reaction experiment [11]. Excitation energies are in keV. The cross-section values given in the second column are the values at approximately the angle of the first maximum of the angular distribution, for $l = 0$ and 1: 6° ; for $l = 2$: 13° ; for $l = 3$: 16° ; for $l = 4$: 30° ; for $l = 5$: 30° ; for structureless or strongly incomplete angular distributions: 16° or some other angle.

Present					ENSDF		(d, p) reaction [11]		
E_x	$\frac{d\sigma}{d\Omega}(\frac{\mu\text{b}}{\text{sr}})$	L	J^π	$(2j+1)S_{lj}$	E_x	L or J^π	E_x	L or J^π	$(2j+1)S_{lj}$
0	2122(26)	0	$1/2^+$	0.47	0	$1/2^+$	0	$1/2^+$	≈ 0.36
12.3	1859(27)	2	$3/2^+$	1.13	12.322(5)	$3/2^+$	12(5)	$3/2^+$	≈ 1.20
288.3	2958(40)	5	$11/2^-$	2.30	288.247(9)	$11/2^-$			
					291.174(9)	$(5/2)^+$	294(5)		
302.8	330(7)	2	$3/2^+$	0.19	302.366(7)	$3/2^+$			
					539.786(13)	$1/2^+$	500(5)	$1/2^+$	≈ 0.02
576.6	22(1)	(4)	$(7/2^+)$	0.12	577.546(12)	$(7/2)^+$			
630.8	515(9)	2	$5/2^+$	0.30	630.559(10)	$3/2^+, 5/2^+$	629(10)	2	0.35
674.3	87(4)	2	$3/2^+$	0.03	676.478(12)	$(3/2, 5/2)^+$	679(10)		
791.1	283(6)	3	$7/2^-$	0.18	794(10)	3	794(10)	$5/2^-, 7/2^-$	0.24
858.5	397(7)	2	$3/2^+$	0.24	858.496(11)	$3/2^+, 5/2^+$	858(10)	$1/2^-, 3/2^-$	0.11
					862.76(9)	+			
					883.34(5)	$(9/2)^+$			
886.0	195(5)	2	$5/2^+$	0.12	887.108(10)	$3/2^+, 5/2^+$	888(10)	(1)	(0.03)
					923.943(9)	$3/2^+, 5/2^+$			
969.4	6.0(10)				968.8(6)	$15/2^-$			
					1021.577(23)	$3/2^+, 5/2^+$			
1066.8	2.8(7)								
1111.2 ^a	4.9(10)	3	$5/2^-, 7/2^-$	0.004, 0.003	1112.335(11)	$3/2^+, 5/2^+, 7/2^+$			
1211.1	1.9(3)				1211.784(12)	$3/2^+, 5/2^+$			
1247.7	433(10)	0	$1/2^+$	0.10	1247(10)	$1/2^+$	1247(10)	$1/2^+$	≈ 0.07
1271.3	2786(45)	3	$7/2^-$	1.63	1273(10)	$5/2^-, 7/2^-$	1273(10)	$7/2^-$	≈ 1.95
1283.6	1456(32)	1	$3/2^-$	0.52	1283.96(3)	$(3/2)^-$	1286(10)	$3/2^-$	≈ 0.66
1329.5 ^a	233(12)	3	$7/2^-$	0.14	1329.329(17)	$(5/2)^+$	1326(10)	(3)	(0.19)
					1352.68(5)	$(5/2, 7/2)^+$			
1501.5	9(3)								
					1528.63(9)	$3/2^+, 5/2^+$			
					1532.38(8)				
1563.6	96(6)	2	$5/2^+$	0.05	1563.380(23)	$(3/2^+, 5/2^+)$			
1582.7	589(12)	1	$1/2^-$	0.14	1581(10)	$1/2^-, 3/2^-$	1581(10)	$1/2^-$	0.21
1616.1	33(3)				1620.505(24)	$(3/2^+, 5/2^+)$	1615(10)?		
1689.3	3.9(5)				1689.63(5)				
1704.7	1.7(25)				1706.89(5)	$3/2, 5/2^+$			
1770.9 ^a	366(10)	3	$5/2^-$	0.27	1769.69(5)	$3/2, 5/2^+$	1770(10)	$5/2^-, 7/2^-$	0.34
					1770(10)	3			
1833.7	41(4)				1830.29(24)	$3/2, 5/2^+$			
1872.4	41(3)								
1938.3	42(2)								
1968.2	110(7)	3	$7/2^-$	0.05					
2017.0	52(6)								
2025.1	108(7)				2026(20)		2026(20)		
2075.8	96(6)	1	$3/2^-$	0.02					
2101.3	14(3)								
2113.4	81(6)	1	$3/2^-$	0.02					

Table 1. Continued.

Present data					ENSDF [8]		(d, p) reaction [11]		
E_x	$\frac{d\sigma}{d\Omega}(\frac{\mu\text{b}}{\text{sr}})$	L	J^π	$(2j+1)S_{lj}$	E_x	L or J^π	E_x	L or J^π	$(2j+1)S_{lj}$
					2115(20)	(2)	2115(20)	(5/2 ⁺)	(0.11)
2142.2	61(4)	(3)	(7/2 ⁻)	0.03					
2171.2	137(7)	3	5/2 ⁻	0.08	2171(20)	3	2171(20)	3	≈ 0.06
2223.0	13(2)								
2245.3	21(3)								
2266.9	26(4)								
2288.1	92(5)	3	7/2 ⁻	0.01					
2325.3	115(7)								
2338.8	92(6)								

^a Possible doublet.**Table 2.** Parameters of the optical-model potentials for the entrance and exit channels, and of the neutron binding potential. A finite-range parameter FNRNG = 0.621 was used in the DWBA calculations [20].

	d	p	n
V_r (MeV)	113.6	52.64	^a
$4W_D$ (MeV)	59.67	32.40	
W_0 (MeV)		3.67	
V_{is} (MeV)	6.61	6.20	$\lambda = 25$
r_r (fm)	1.17	1.18	1.17
r_0 (fm)		1.12	
r_w (fm)	1.32	1.12	
r_{ls} (fm)	1.16	1.01	
r_c (fm)	1.15	1.25	
a_r (fm)	0.75	0.67	0.75
a_0 (fm)		0.62	
a_w (fm)	0.85	0.62	
a_{ls} (fm)	0.66	0.75	
Non-local	0.54	0.85	

^a Depth fitted for each state by CHUCK3.

computer programme CHUCK3 [20]. The optical-model parameters used to calculate the distorted waves in the entrance and exit channels, as well as those of the neutron potential well, are given in table 2. Finite-range and non-locality corrections with standard parameters for a (d, p) reaction were employed, as also specified in table 2. There are many recommended optical-model parameter sets in the literature [21] and, as discussed below, we have examined several possibilities. The parameters from table 2 were chosen starting from those of refs. [22] (for deuteron) and [23] (for proton), in such a way to reproduce best the shapes of both the angular distribution and asymmetry for states with representative l, J values, but taking care that their values stay within accepted limits. As can be seen in fig. 2, angular distributions with the same l have similar shapes, thus being insensitive to the J values (where J may take the values $l + 1/2$ or $l - 1/2$). In measurements

with a polarized beam, one can use the analyzing power which is sensitive to the J value —this can be seen in fig. 2 for the levels 631 keV, assigned as $5/2^+$, and 674 keV, assigned as $3/2^+$, and also for the 1111 keV level where both calculations are shown. Thus, for most of the levels with a sufficient amount of data points, the ambiguity $J = l \pm 1/2$ can be resolved using the analyzing power. This type of complete analysis could not be done either for the levels which were obscured by impurity peaks at too many angles, or for levels with structureless angular distribution (which are generally weakly populated levels, probably not excited in a direct transfer, but rather by a multi-step process). As can be seen in fig. 2, the experimental data for most of the states are well reproduced by the calculations, indicating the dominance of a direct, one-step mechanism.

Some comments below concern particular levels from table 1. We could not observe the 291.2 keV, $(5/2)^+$ level [8], because it was probably very weakly excited in our reaction, and difficult to resolve from the much stronger 288 keV and 302 keV peaks (fig. 1). The later two levels were observed with the known characteristics of $J^\pi = 11/2^-$ and $3/2^+$ [8], respectively. The weak increase at forward angles observed for the cross-section of the 288 keV level might be due to the $l = 2$ contribution of the 291 keV level. The 539.8 keV, $1/2^+$ level [8] was also not observed. The same holds for other levels with low spins (883, 924, 1353, 1529, 1620 keV, etc., see table 1). For the 576.6 keV level, both the large orbital angular momentum (very likely $l = 4$ but not too well described by the DWBA) and the $J = 7/2$ value (see the analyzing power) are confirmed. There are a few levels for which our assignment differs from the previous ones. Thus, we found a level with $E_x = 1111.2$ keV, and clear $l = 3$ assignment, which is very close to a previously known level at $E_x = 1112.3$ keV that was assigned as $3/2^+, 5/2^+, 7/2^+$. It might be that there is a doublet at this energy. Other two possible doublets were suggested in the ENSDF compilation [8] (see table 1): at 1329.5 keV, for which we assign, as in [11] $J^\pi = 7/2^-$, in agreement with the ($l = 3$) value from the older (d, p) experiment, that could be very close to a positive-parity level; similarly, the 1770.9 keV level, for which we assign $J^\pi = 5/2^-$, again in agreement with

the older (d, p) experiment, might be almost degenerate in energy with a positive-parity level.

The main result of our analysis is a reliable determination of the level scheme below 1 MeV, by the unambiguous determination of the spin of the levels at 631, 675, 858, and 886 keV (table 1, fig. 2). Many other unambiguous J^π assignments were also made for levels above 1.0 MeV. Above 1.5 MeV mostly negative-parity levels were observed.

For the levels where the comparison with the DWBA prediction was good, the spectroscopic factors were determined from the normalization of the theoretical cross-section to the data points, as $S_{lj} = \sigma_{exp}/\sigma_{DWBA}$. The absolute cross-sections in fig. 2 and table 1 were determined by using a nominal target thickness of $60 \mu\text{g}/\text{cm}^2$ as determined by monitoring the ion current of the mass separator. We assume an accuracy of 10–15% of the target thickness, which gives a measure of the systematic error of the determined spectroscopic factors. The deduced spectroscopic factors may also depend on the optical-model parameters used for the reaction channels. We have investigated this effect by combining different potentials for the deuteron and proton channels, recommended in the RIPL-2 database [21]. Thus, in addition to the potentials from refs. [22, 23], we have also considered for the deuteron the potential parameters from [24, 25], and for the proton those of [26]. Calculations were made with combinations of these potentials, and spectroscopic factors were extracted whenever the shape of the angular distribution was reasonably described (which was mostly the case). In general, no radial cut-off was found necessary in order to improve the description of the data. It was found that the spectroscopic factors differed by those from table 1 by at most 15% (for $l = 0, 2$, and 3) and only in the $l = 5$ case variations as large as 20% were found. Consequently, we may assume that this type of uncertainty is typically 15%. A further question concerns the effect of the deuteron breakup on the extracted spectroscopic factors. For the (d, p) reaction on light targets this was recently studied in ref. [27]. In order to estimate these breakup effects, we performed continuum discretized coupled channels (CDCC) calculations for some of our transitions. In the CDCC method [28, 29] the continuum states which contribute to the transfer are described by a finite number of discretized momentum bins $[k_i, k_{i+1}]$ up to some maximum momentum k_{max} and angular momentum L_{max} . The calculations were carried out with the computer code FRESKO [30]. The proton target and neutron target potentials necessary to generate the deuteron target potential were chosen starting from the Becchetti-Greenlees potentials [23] at an energy equal to half the beam energy, slightly re-adjusted to describe the deuteron elastic scattering calculated with the potential used in the DWBA case. Figure 3 illustrates the results of these calculations in which only the coupling to the $L = 0$ continuum was included, the contribution from higher L values being found negligible at the forward angles measured in our case. As can be seen in this figure, the CDCC predictions agree reasonably well to those of the DWBA, both in shape and absolute value. The effects on the extracted spectroscopic factors are found to depend

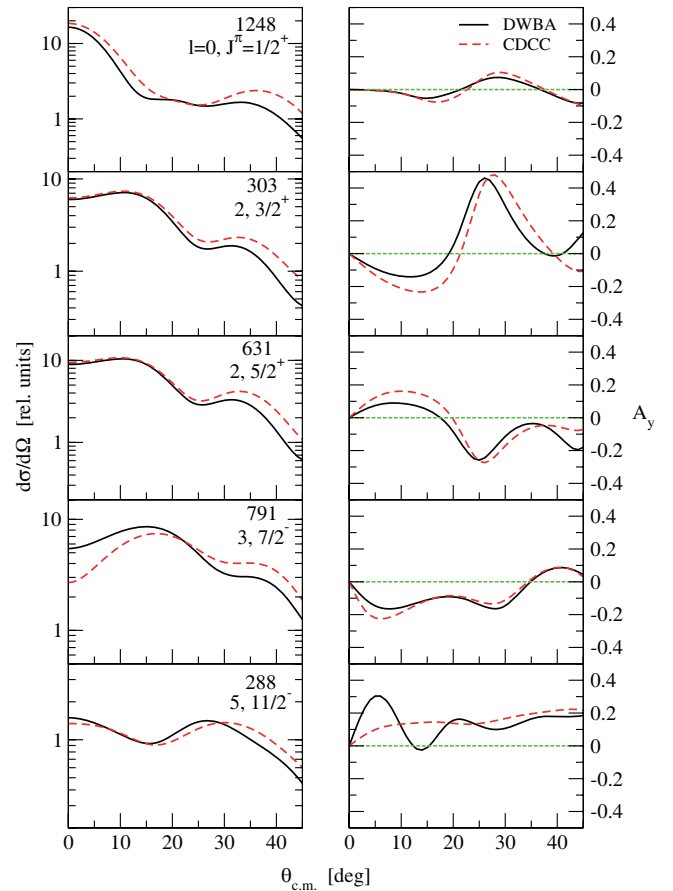


Fig. 3. Results of the CDCC calculations performed with the code FRESKO, compared to the DWBA ones (spectroscopic factors assumed as 1 in both cases), for several selected states (labeled by their excitation energy in keV, and the l and J^π quantum numbers). See text for details.

on the transferred angular momentum, *e.g.*, the extracted S_{lj} decrease for $l = 0$ and 2 and increase for $l = 3$, the variations found being within 20%. Consequently, taking into account the sources of error for the spectroscopic factors derived from the DWBA analysis, due to both the optical model potentials and the deuteron breakup effects, we estimate an overall uncertainty in the derived spectroscopic factors of the order of 25%.

In table 1 one can observe that our spectroscopic factors agree reasonably well with those deduced in the previous (d, p) reaction measurement of ref. [11]. Summing the spectroscopic strength $(2j + 1)S_{lj}$ for each l, j pair of values one finds the number of neutron holes for each shell model orbital. For the five orbitals of the 50–82 major shell one thus finds the values 0.57 ($s_{1/2}$); 1.59 ($d_{3/2}$); 0.47 ($d_{5/2}$); 0.12 ($g_{7/2}$); 2.30 ($h_{11/2}$).

3 Discussion

Figure 4 presents the evolution of the low-lying positive-parity states in odd- A $^{129-137}\text{Ba}$ isotopes and in $N = 77$ isotones around ^{133}Ba . It is conspicuous that along both

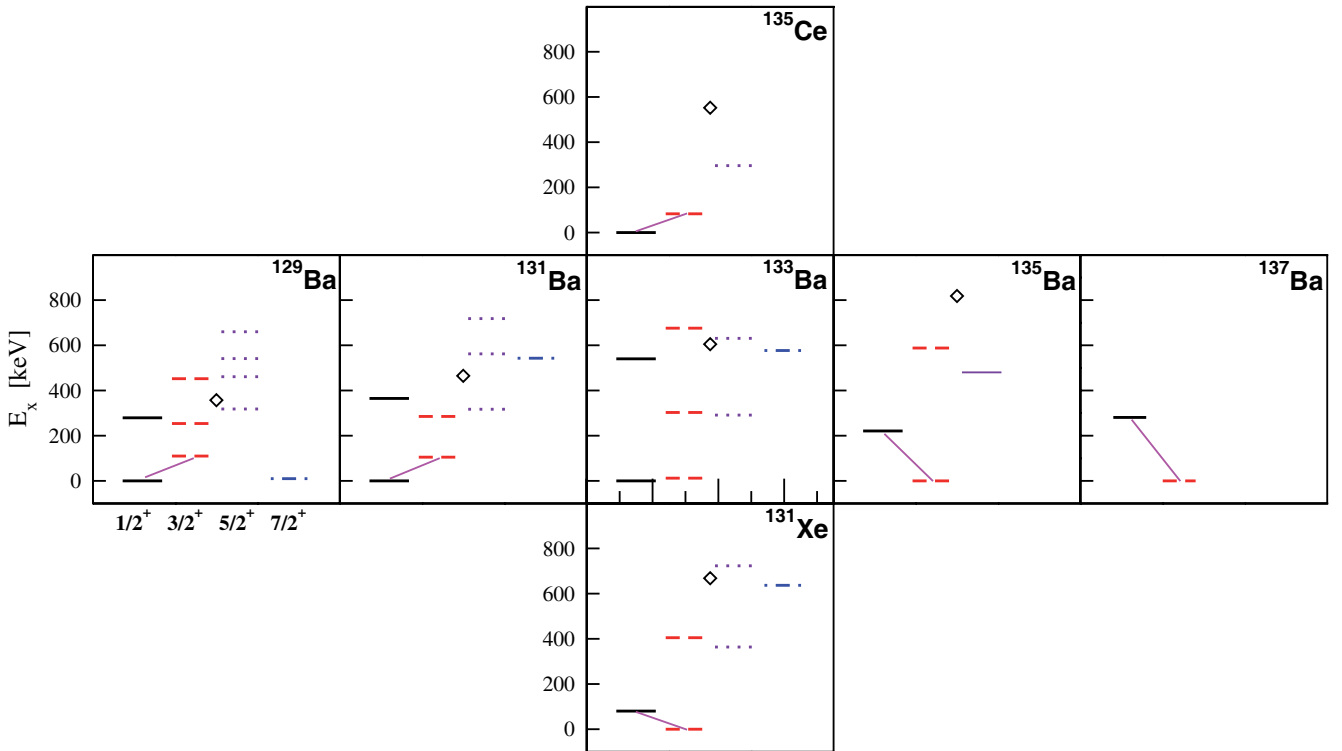


Fig. 4. The evolution of the experimental low-lying positive-parity states in the Ba isotopes and the $N = 77$ isotones around ^{133}Ba . The diamonds show the position of the 2_1^+ level in the Ba even-even cores with one neutron more.

the Ba and $N = 77$ chains the lowest $1/2^+$ and $3/2^+$ states cross each other, with ^{133}Ba being the point where the two states are almost degenerate (only 12 keV difference).

3.1 IBFM calculations

At low excitation energies, ^{133}Ba can be regarded as one fermion (neutron hole) coupled to the nearly- $E(5)$ ^{134}Ba core. In fig. 5, we compare the experimental spectrum with three theoretical predictions within the IBFM (Interacting Boson-Fermion Model) framework [31]. All calculations discussed were performed with the codes PHINT and FBEM (which calculate energy levels and electromagnetic transition probabilities for the even-even nuclei within the IBM-1) [32], and ODDA, PBEM, and SPEC (for calculating energy levels, transition probabilities, and one-nucleon-transfer spectroscopic factors for odd- A nuclei within the IBFM) [33]. The first level sequence shown on the left side of fig. 5 is the one predicted by the supersymmetrical $E(5/4)$ scheme [5], which corresponds to the coupling of one $d_{3/2}$ particle to a core with an $E(5)$ critical point symmetry. The $E(5/4)$ solution proposed in ref. [5], is an analytical one, and corresponds to a special boson-fermion interaction. In ref. [34] the behaviour at the critical point is discussed within the IBFM. The Hamiltonian of the odd-mass nucleus is

$$H = H_B + H_F + V_{BF}, \quad (1)$$

where H_B is the boson Hamiltonian of the even-even core, H_F is the single-particle Hamiltonian, and V_{BF} the

boson-fermion interaction. For the part which describes the even-even core one chooses the form

$$H_B = x\hat{n}_d + \frac{1-x}{N}\hat{Q}_B \cdot \hat{Q}_B, \quad (2)$$

where for x varying between 1 and 0, one covers the evolution between the $U(5)$ and $O(6)$ symmetries (here, $\hat{Q}_B = s^\dagger\tilde{d} + \tilde{s}d^\dagger$, therefore $\chi = 0$, in order to preserve the $O(5)$ symmetry). The $E(5)$ critical point corresponds to the value $x = \frac{4N-8}{5N-8}$. The boson-fermion interaction is restricted to a quadrupole-quadrupole term of the form

$$V_{BF} = -2\frac{1-x}{N}\hat{Q}_B \cdot \hat{q}_F, \quad (3)$$

which preserves the $spin^{BF}(5)$ symmetry for any value of x [34]. For the ^{134}Ba core (number of bosons $N = 5$), the $E(5/4)$ scheme corresponds to the value $x = 0.706$. The appropriate $E(5/4)$ strength of the quadrupole-quadrupole interaction (3) is found to correspond to a value $BFQ = 0.207$ for the strength parameter of the quadrupole-quadrupole interaction in the input of the ODDA code (which uses a semi-microscopic parameterization for the boson-fermion interaction that comprises three terms: monopole, quadrupole, and exchange [33,35]). The resulting usual $E(5/4)$ level scheme (scaled such that the energy of the first multiplet lies at 500 keV) is shown as scheme (a) in fig. 5, and it consists of typical degenerated multiplets, with the $3/2^+$ state lacking from the first multiplet and appearing higher [5,34]. The experimental level scheme presents level groups, which resemble these

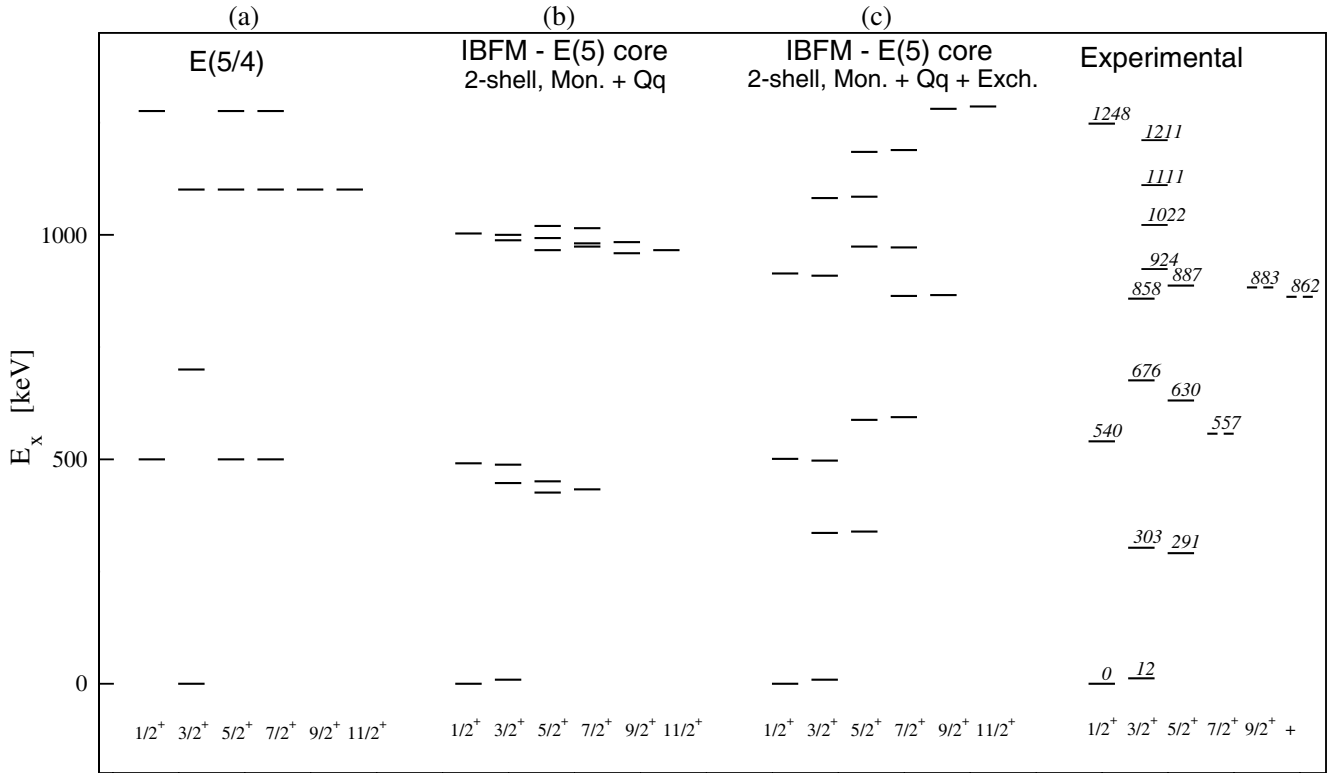


Fig. 5. The low-energy positive-parity levels of ^{133}Ba compared to different theoretical schemes. The experimental states at 924, 1022, 1111, and 1211 keV are not yet resolved and have $J^\pi = 3/2^+$ or $5/2^+$. (a) the $E(5/4)$ scheme (scaled such that the first multiplet has an energy of 500 keV); (b) IBFM calculation with the odd nucleon occupying two almost degenerated $s_{1/2}$ and $d_{3/2}$ orbitals, and a quadrupole-quadrupole boson-fermion interaction with the strength equal to that used in the $E(5/4)$ scheme ($BFQ = 0.206$, which corresponds to the critical point $E(5/4)$ [34]), and a monopole-monopole interaction strength $BFM = -0.25$; (c) same as (b) but with an exchange force with the strength parameter $BFE = 0.50$ added. See text for other details.

multiplets with broken energy degeneracy (large anharmonicities), but the most severe discrepancy between this highly idealized level scheme and the experiment is that there are more experimental levels. Actually, the experimental level scheme indicates strongly that it is dominated by both $d_{3/2}$ and $s_{1/2}$ orbitals: there is a $1/2^+$, $3/2^+$ doublet near the ground state, and the levels between 290 and 676 keV suggest multiplets resulting from the coupling between these two orbitals and the 2^+ state (605 keV) of the core.

The IBFM calculations discussed next included more than one orbital for the odd fermion. For the multi-shell case, quasi-particle energies and occupancies were required for the implied orbitals. We generated these by starting from the single-particle energies of Reehal and Sorensen [36], where we readjusted the energies of the $s_{1/2}$ and $d_{3/2}$ orbitals such that they are almost degenerated (~ 30 keV difference instead of 280 as given by the parameterization). This was required by the small energy difference of 12 keV between the $1/2^+$ g.s. and the $3/2^+$ states (table 1). The quasi-particle energies and occupancies were then provided by a BCS calculation (with a pairing gap $\Delta = 12A^{-1/2}$), for all five orbitals in the 50–82 shell: $g_{7/2}$, $d_{5/2}$, $s_{1/2}$, $d_{3/2}$, and $h_{11/2}$. This procedure gives realistic shell occupancies, which compare

well with those found from the spectroscopic factors of the present (d, p) reaction measurements (see the end of sect. 2.2). The numbers of holes in each of these orbitals, calculated as $(2j+1)(1-v_j^2)$ (where v_j^2 is the orbital occupancy), are 0.64 ($s_{1/2}$), 1.28 ($d_{3/2}$), 0.57 ($d_{5/2}$), 0.37 ($g_{7/2}$), 2.06 ($h_{11/2}$).

We performed first an IBFM calculation which included only the two orbitals $s_{1/2}$ and $d_{3/2}$, and again only the quadrupole ($Q \cdot q$) boson-fermion (BF) interaction, with the same strength as that used in the $E(5/4)$ calculation ($BFQ = 0.207$). To compare with the experiment, a monopole term [31] (which mainly changes the energy scale) with strength $BFM = -0.25$ [33] was added. The result is shown in the level scheme (b) in fig. 5. One gets nearly degenerated multiplets, which, nevertheless, compare well with the experiment in centroids, number of levels, and spin values. However, the splitting of these multiplets is too small and almost independent on the BF quadrupole strength. A more realistic splitting of these multiplets can be obtained by adding the third usual term of the BF interaction, the exchange force [35,33]. The level scheme (c) in fig. 5 shows the result of such a calculation with the monopole and quadrupole strength parameters kept as before, and an exchange force strength parameter $BFE = 0.50$ [33]. Now the calculated level scheme shows

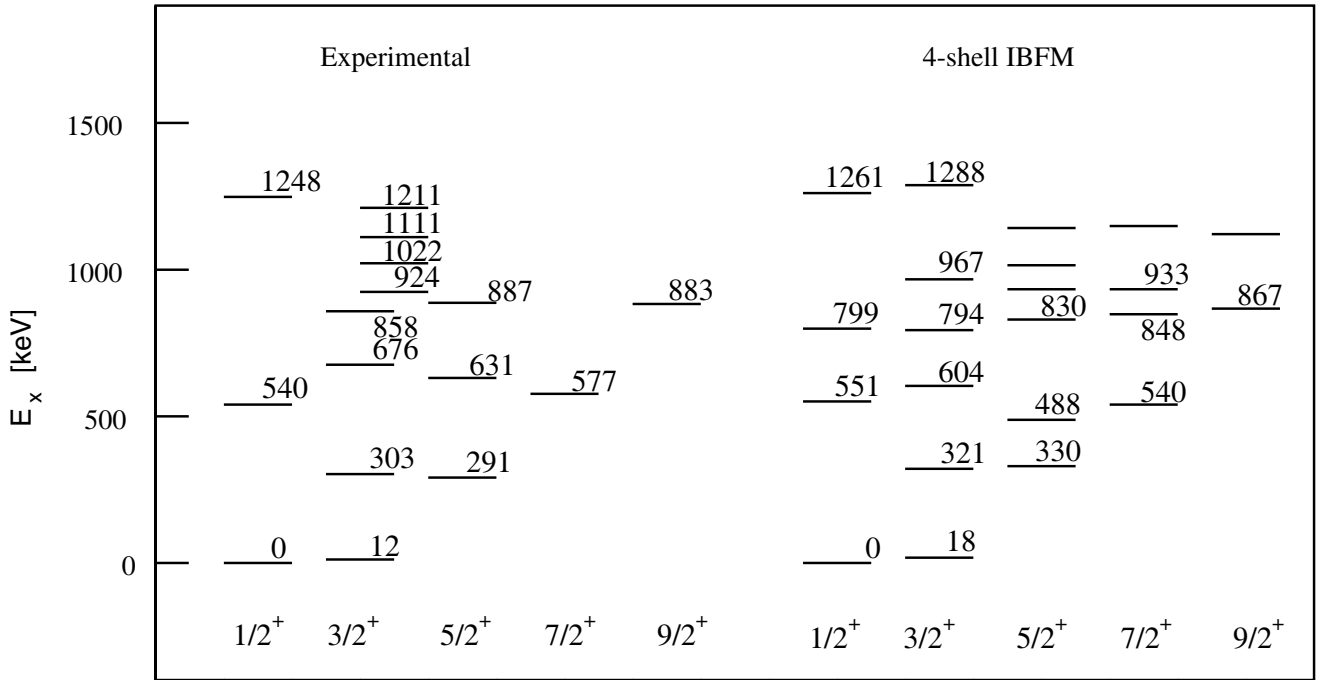


Fig. 6. Comparison between experimental and a four-shell IBFM calculations. The IBA-1 parameters of the core were determined such as to describe the ^{134}Ba level scheme. The BF interaction strengths are the same as in the two-shell case (fig. 5(c)): BFM , BFQ , $BFE = -0.25, 0.20, 0.50$.

a much better similarity with the experimental one, including the multiplet with many states spread between 850 and 1250 keV.

Until now all IBFM calculations used an $E(5)$ core, which is known to be a reasonably good description of ^{134}Ba [3], and only the $(s_{1/2}, d_{3/2})$ fermionic space. One more IBFM calculation was performed using an IBA-1 parameterization that fits the detailed properties of the ^{134}Ba core [37] and allowing the odd nucleon to occupy all four positive-parity orbitals available in the 50–82 shell ($g_{7/2}$, $d_{5/2}$, $s_{1/2}$, and $d_{3/2}$). The IBA-1 model parameters, which describe the ^{134}Ba core are (in the notations of the PHINT input [32]) $HBAR = 0.553$, $C(0, 2, 4) = 0.80$; -0.027 ; 0.146 , $F = 0.043$, and $G = -0.092$ [37]. For these IBFM calculations, the BF strength parameters were as above: $BFM = -0.25$, $BFQ = 0.207$, and $BFE = 0.50$. The results are shown in fig. 6, where an overall good agreement with the experimental level scheme can be observed. One should note that the IBFM strength parameters found as adequate in these calculations are rather similar with those used in the description of the Te isotopic chain with $N = 65$ to 77 [38] (BFM between -0.1 and -0.28 , $BFQ = 0.20$, and $BFE = 0.95$).

So far we have compared only the experimental and calculated level schemes. A more complete estimation of the quality of the theoretical description must include other experimental data as well, among which absolute electromagnetic decay probabilities (or transition strengths) are essential. In particular, among the fingerprints of the critical-point symmetries are not only the energy ratios but also the quadrupole transition $B(E2)$ values [3, 5, 34]. Unfortunately, level lifetimes are

not known in ^{133}Ba (except for the isomeric states $3/2^+$, 12 keV, and $11/2^-$, 288 keV [8]). Therefore, we compare the experimental branching ratios and the spectroscopic factors with the calculated ones. For this, we calculated both $E2$ and $M1$ transitions. The parameters entering the $E2$ and $M1$ transition operators were determined by fitting the known transition probabilities and branching ratios in the ^{134}Ba core [37]. In the notations of the input of the FBEM [32] and PBEM [33] programs, these parameters are as follows. For the $E2$ transitions the effective charge $E2SD = 0.13$ (in units of eb), and $E2DD = 0$ for the $E(5)$ case (corresponding to $\chi = 0$) or $E2DD = -0.067$ (corresponding to $\chi = -0.52$, found by transforming the general IBM-1 Hamiltonian parameterization given above to its multipole expansion form). In the odd- A case, one adds a fermion quadrupole effective charge, which was taken $EFF = 0.13$. For the $M1$ transitions, we use the parameter values $M1 = 0.21$ and $M1E2 = 0.20$, and in addition, the odd fermion gyromagnetic factors $g_l = 0$, $g_s = -2.6789\mu_N$ (*i.e.*, the free value quenched by a factor of 0.7).

Table 3 gives the IBFM wave function compositions of the lowest states in the level scheme, as well as the experimental and calculated branching ratios for the two-shell plus the $E(5)$ -core (fig. 5(c)), and the four-shell fitted-core IBFM calculations (fig. 6). Looking at the wave functions, it can be seen that for these lowest states, the two-shell approximation ($s_{1/2}$, $d_{3/2}$) is not too bad, since in the four-shell calculation the added orbitals $d_{5/2}$ and $g_{7/2}$ do not enter into the structure of these states by more than about 10%. The main decay modes are reasonably reproduced with the two-shell calculation failing mainly in the

Table 3. Comparison between the experimental [8] and IBFM calculated electromagnetic decay branching ratios, for the low-lying positive-parity levels of ^{133}Ba . The numbers given for the wave functions represent the percentages of the orbitals, in the order $s_{1/2}$, $d_{3/2}$ (plus $d_{5/2}$ and $g_{7/2}$ in the four-shell case). The subscript to the spin number is the order number of the level with that spin, which coincides with that of the IBFM calculations (figs. 5, 6). Only branches above 4 (relative to the strongest which is taken as 100) are given.

E_i (keV)	J_i^π	IBFM wave function %		J_f^π	Exp. BR	Calculated BR	
		2-shell	4-shell			2-shell	4-shell
0	$1/2_1^+$	89,11	93,3,4,0				
12	$3/2_1^+$	6,94	2,96,1,1	$1/2_1^+$	100	100	100
291	$5/2_1^+$	24,76	24,74,1,1	$1/2_1^+$	17.5	26	39
				$3/2_1^+$	100	100	100
303	$3/2_2^+$	52,48	49,48,2,1	$1/2_1^+$	100	97	100
				$3/2_1^+$	86	100	77
540	$1/2_2^+$	9,91	1,87,10,2	$1/2_1^+$	–	100	1
				$3/2_1^+$	100	23	100
				$3/2_2^+$	–	6	62
577	$7/2_1^+$	10,90	2,94,1,3	$3/2_1^+$	100	100	100
				$5/2_1^+$	5.6	11	23
631	$5/2_2^+$	64,36	64,24,12,0	$1/2_1^+$	17	67	23
				$3/2_1^+$	100	100	100
				$5/2_1^+$	5.0	58	30
				$3/2_2^+$	3.6	54	27
676	$3/2_3^+$	43,57	43,47,7,3	$1/2_1^+$	29	100	100
				$3/2_1^+$	100	90	90
				$5/2_1^+$	82	24	52
				$3/2_2^+$	8.8	43	99

Table 4. Comparison between the experimental (table 1) and IBFM calculated spectroscopic factors in the (d, p) reaction for the low-lying positive-parity levels of ^{133}Ba . The subscript to the spin number is the order number of the level with that spin which coincides with that of the IBFM calculations (figs. 5, 6).

E_x (keV)	J^π	$(2j+1)S_{lj}$		
		Exp.	2-shell	4-shell
0	$1/2_1^+$	0.47	0.44	0.49
540	$1/2_2^+$	–	0.15	0.02
1248	$1/2_3^+$	0.10	0.03	0.001
12	$3/2_1^+$	1.13	0.87	1.00
303	$3/2_2^+$	0.19	≈ 0	≈ 0
676	$3/2_3^+$	0.03	0.32	0.10
858	$3/2_4^+$	0.24	0.05	0.002
291	$5/2_1^+$	–	0	≈ 0
631	$5/2_2^+$	0.30	0	0.01
886	$5/2_3^+$	0.12	0	0.16
577	$7/2_1^+$	0.12	0	0.01

case of the $1/2_2^+$, 540 keV state. The situation of this state, as well as that of the $5/2_2^+$, 631 keV and $3/2_3^+$, 676 keV states improves in the four-shell calculation. Also, in the two-shell case the $5/2^+$ and $7/2^+$ states have zero spectroscopic factors.

In table 4, we compare the experimental spectroscopic factors with the IBFM calculated ones. The large spectroscopic factors of the $1/2_1^+$ (g.s.) and $3/2_1^+$ (12 keV) states are nicely reproduced, which confirms their single-particle state nature (see also their structure in table 2). Although, as remarked above, the spectroscopic strengths summed over the different orbitals are in reasonable agreement with the theoretical values (which are actually fixed by the BCS calculation), the fragmentation of the orbital single-particle strengths on the different excited states is not too well reproduced (table 4). This indicates that more intricate wave functions may be needed.

3.2 Shell model calculations

In order to understand in more detail the structure observed in this nucleus, we performed spherical-shell model calculations. These calculations were performed with the NuShellX code [39]. Both protons and neutrons span the same orbitals, $1g_{7/2}$, $2d_{5/2}$, $2d_{3/2}$, $3s_{1/2}$, and $1h_{11/2}$.

The realistic effective interaction in this orbital space was obtained starting from the CD-Bonn-2000 nucleon-nucleon potential [40] and using a G -matrix renormalization followed by the \hat{Q} -box method for summing up all non-folded diagrams to the third order and all folded diagrams to infinite order [41]. An harmonic-oscillator basis with $\hbar\omega = 7.87$ MeV was used for describing the radial part of the single-particle wave functions. The values of

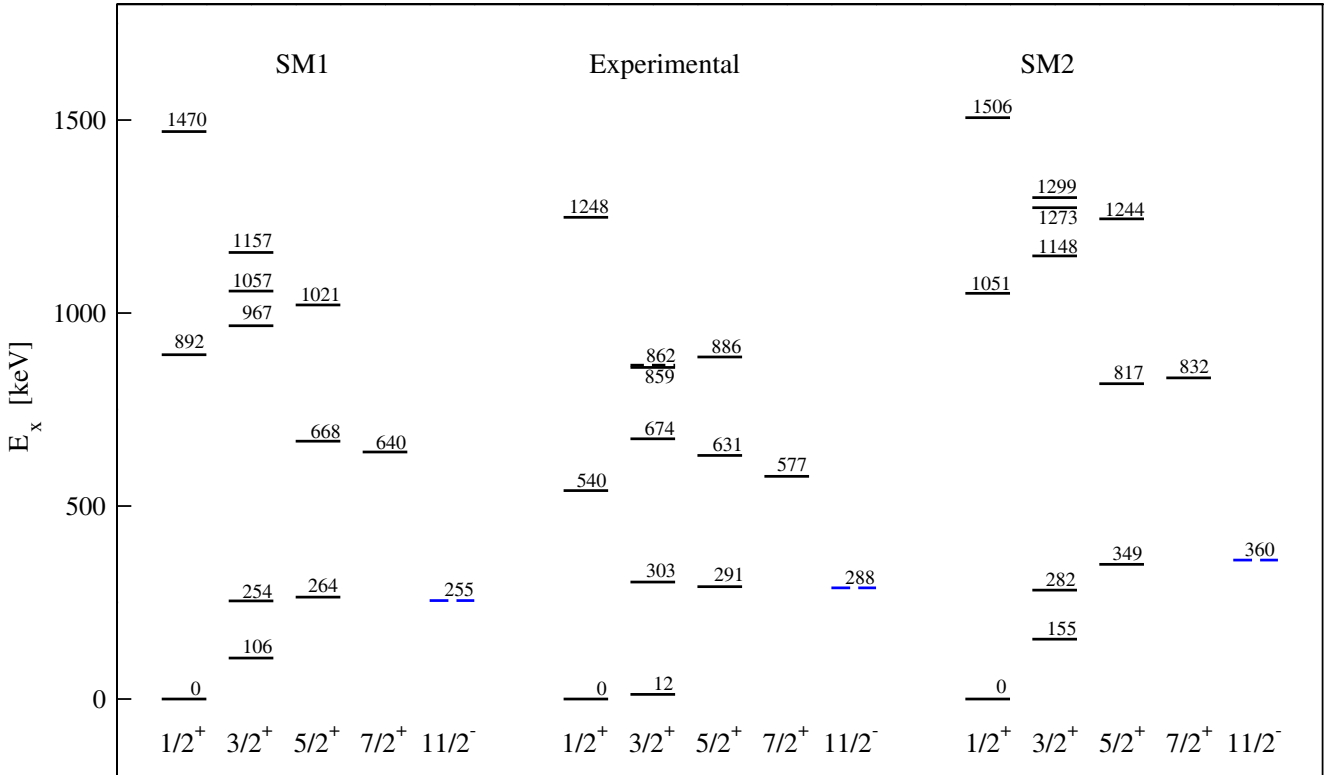


Fig. 7. Comparison between the shell model calculated and experimental low-energy level scheme of ^{133}Ba (levels with both parities).

the effective single-particle energies, relative to the $g_{7/2}$ orbitals, were $e_{d_{5/2}}^\pi = 0.962$, $e_{d_{3/2}}^\pi = 2.440$, $e_{s_{1/2}}^\pi = 2.340$, $e_{h_{11/2}}^\pi = 2.792$, $e_{d_{5/2}}^\nu = 1.236$, $e_{d_{3/2}}^\nu = 2.990$, $e_{s_{1/2}}^\nu = 3.055$, and $e_{h_{11/2}}^\nu = 3.105$ and they were estimated based on the energy levels in ^{131}Sn (for neutrons) and ^{133}Sb (for protons). Excitation energies were calculated for a few “key” nuclei (^{130}Sn , ^{134}Te , ^{132}Sb , and ^{134}Te) and they compared well to the experimental data.

The effective charges $\tilde{e}^\pi = 1.5$ and $\tilde{e}^\nu = 0.5$ were employed for the calculation of the $B(E2)$ reduced transition probabilities, while the g factors $\tilde{g}_i^\pi = 1.0$, $\tilde{g}_i^\nu = 0.0$, $\tilde{g}_s^\pi = 5.586$, and $\tilde{g}_s^\nu = -3.826$ were used for estimating the $B(M1)$ transition probabilities.

For practical reasons, the total configuration space was truncated to manageable m scheme basis dimensions by taking into account the fact that the $d_{3/2}$, $s_{1/2}$, and $h_{11/2}$ orbitals are rather well separated by a relatively high-energy gap from the lower orbitals $g_{7/2}$ and $d_{5/2}$. The logical truncation criteria were as follows:

- at most one- or two-neutron holes were allowed in the lower orbitals $g_{7/2}$ and $d_{5/2}$, respectively. $[(N_{g_{7/2}}^\nu = 8 \wedge N_{d_{5/2}}^\nu \geq 4) \vee (N_{g_{7/2}}^\nu = 7 \wedge N_{d_{5/2}}^\nu = 6)]$;
- at most four or two protons were allowed to “jump” from the lower orbital $g_{7/2}$ into the $d_{5/2}$ orbital or into the higher ones ($d_{3/2}$, $s_{1/2}$, and $h_{11/2}$), respectively $[(N_{g_{7/2}}^\pi \geq 2 \wedge N_{d_{3/2}}^\pi + N_{s_{1/2}}^\pi + N_{h_{11/2}}^\pi = 0) \vee (N_{g_{7/2}}^\pi \geq 4)]$;
- for ^{133}Ba , the allowed spin values for proton and neutron subconfigurations were $J^\pi \leq 6$ and $J^\nu \leq 23/2$,

respectively. For ^{132}Ba , the maximum $J^{\pi,\nu}$ limits were 6 and 10 for protons and neutrons, respectively.

Even though the truncation scheme provided relatively large basis dimensions ($< 2 \times 10^6$), the truncation was rather severe and in order to compensate at some extent for the missing configurations, the “pairing” interaction matrix elements, $\langle jj | V_{J=0}^{\pi,\nu} | jj \rangle$, were made more attractive so that the excitation energy spectra of ^{138}Ba (for protons) and $^{126,128}\text{Sn}$ (for neutrons) are described adequately. These “pairing” corrections are equivalent to global increases in the $\pi\pi$ and $\nu\nu$ pairing strengths $\Delta G^{\pi\pi} = 66.2$ and $\Delta G^{\nu\nu} = 126.8$ keV, respectively $[\langle jj | \Delta V_{J=0} | jj \rangle = -(2j+1)/2 \cdot \Delta G]$. The set of results obtained with the unmodified interaction is referred in the text as SM1, while the calculations performed with the “pairing”-corrected interaction are labeled SM2.

In the following, we compare the results of the predictions with the experimental data. Figure 7 shows a comparison of the low-spin positive-parity levels (the lowest levels with $J^\pi = 1/2^+$, $3/2^+$, $5/2^+$, and $7/2^+$) with the predictions of the calculations with the two effective interactions used; the lowest negative-parity level $11/2^-$ is also included. Although the spectrum predicted by the SM1 interaction is more compressed than that of the SM2 interaction, the properties of the levels predicted by the later (such as the decay modes and spectroscopic factors, discussed below) compare better to the experimental ones. Table 5 gives the main composition of the wave functions of the low-lying positive-parity states and one can see that

Table 5. Main components of wave functions of the states in ^{133}Ba , calculated with the SM2 effective interaction. Configurations with percentages (p) greater than 10% are listed for each state. The average numbers of protons (π) and neutrons (ν) in each orbital are shown between round brackets ($N_{g_{7/2}}, N_{d_{5/2}}, N_{d_{3/2}}, N_{s_{1/2}}, N_{h_{11/2}}$). The partial angular momenta are separately represented for proton and neutron sub-configurations as integer and half-integer subscripts, respectively.

J^π	Occupancy	Config.	p [%]
$1/2_1^+$	$\pi(4.38, 0.98, 0.28, 0.26, 0.11)$	$\pi_0 \otimes \nu_{1/2}$	37
	$\nu(7.95, 5.69, 2.17, 1.21, 9.98)$	$\pi_2 \otimes \nu_{3/2}$	25
$1/2_2^+$		$\pi_2 \otimes \nu_{5/2}$	25
	$\pi(4.90, 0.57, 0.31, 0.20, 0.02)$	$\pi_0 \otimes \nu_{1/2}$	29
	$\nu(7.94, 5.71, 2.09, 1.27, 9.99)$	$\pi_2 \otimes \nu_{3/2}$	28
$1/2_3^+$		$\pi_2 \otimes \nu_{5/2}$	25
	$\pi(4.20, 1.24, 0.24, 0.19, 0.12)$	$\pi_0 \otimes \nu_{1/2}$	29
	$\nu(7.95, 5.51, 2.57, 1.37, 9.59)$	$\pi_2 \otimes \nu_{3/2}$	33
$3/2_1^+$		$\pi_2 \otimes \nu_{5/2}$	20
	$\pi(4.39, 0.96, 0.28, 0.27, 0.10)$	$\pi_0 \otimes \nu_{3/2}$	35
	$\nu(7.93, 5.70, 2.13, 1.27, 9.95)$	$\pi_2 \otimes \nu_{3/2}$	14
		$\pi_2 \otimes \nu_{5/2}$	16
$3/2_2^+$		$\pi_2 \otimes \nu_{7/2}$	12
	$\pi(4.35, 1.02, 0.27, 0.24, 0.11)$	$\pi_0 \otimes \nu_{3/2}$	34
	$\nu(7.94, 5.68, 2.56, 0.88, 9.93)$	$\pi_2 \otimes \nu_{1/2}$	10
		$\pi_2 \otimes \nu_{3/2}$	16
		$\pi_2 \otimes \nu_{5/2}$	12
$3/2_3^+$		$\pi_2 \otimes \nu_{7/2}$	12
	$\pi(4.86, 0.59, 0.32, 0.20, 0.03)$	$\pi_0 \otimes \nu_{3/2}$	26
	$\nu(7.94, 5.73, 2.11, 1.30, 9.92)$	$\pi_2 \otimes \nu_{1/2}$	15
		$\pi_2 \otimes \nu_{3/2}$	14
		$\pi_2 \otimes \nu_{5/2}$	11
$3/2_4^+$		$\pi_2 \otimes \nu_{7/2}$	12
	$\pi(4.80, 0.66, 0.30, 0.22, 0.03)$	$\pi_0 \otimes \nu_{3/2}$	11
	$\nu(7.94, 5.71, 2.23, 1.12, 9.98)$	$\pi_2 \otimes \nu_{1/2}$	16
		$\pi_2 \otimes \nu_{3/2}$	16
		$\pi_2 \otimes \nu_{5/2}$	14
$3/2_5^+$	$\pi(4.57, 0.83, 0.32, 0.24, 0.03)$	$\pi_0 \otimes \nu_{3/2}$	21
	$\nu(7.94, 5.74, 2.59, 1.29, 9.42)$	$\pi_2 \otimes \nu_{3/2}$	17
		$\pi_2 \otimes \nu_{5/2}$	14
		$\pi_2 \otimes \nu_{7/2}$	12
$5/2_1^+$	$\pi(4.33, 1.00, 0.29, 0.28, 0.10)$	$\pi_0 \otimes \nu_{5/2}$	30
	$\nu(7.93, 5.70, 2.29, 1.12, 9.96)$	$\pi_2 \otimes \nu_{1/2}$	13
		$\pi_2 \otimes \nu_{3/2}$	16
		$\pi_2 \otimes \nu_{9/2}$	12
$5/2_2^+$	$\pi(4.25, 1.04, 0.31, 0.33, 0.07)$	$\pi_0 \otimes \nu_{5/2}$	21
	$\nu(7.94, 5.67, 2.46, 0.98, 9.94)$	$\pi_2 \otimes \nu_{1/2}$	11
		$\pi_2 \otimes \nu_{3/2}$	21
$5/2_3^+$	$\pi(4.71, 0.74, 0.29, 0.24, 0.02)$	$\pi_3 \otimes \nu_{1/2}$	15
	$\nu(7.94, 5.71, 2.08, 1.27, 9.99)$	$\pi_3 \otimes \nu_{3/2}$	16
		$\pi_4 \otimes \nu_{3/2}$	13
$7/2_1^+$	$\pi(4.20, 1.06, 0.31, 0.37, 0.07)$	$\pi_0 \otimes \nu_{7/2}$	19
	$\nu(7.93, 5.69, 2.02, 1.37, 9.97)$	$\pi_2 \otimes \nu_{3/2}$	28
		$\pi_2 \otimes \nu_{7/2}$	10
$11/2_1^-$	$\pi(4.09, 1.31, 0.25, 0.25, 0.10)$	$\pi_0 \otimes \nu_{11/2}$	31
	$\nu(7.93, 5.71, 2.66, 1.48, 9.20)$	$\pi_2 \otimes \nu_{11/2}$	12
		$\pi_2 \otimes \nu_{9/2}$	11

Table 6. Branching ratios (b) for low-lying states in ^{133}Ba , predicted by the two shell model calculations, compared to the corresponding experimental values. The calculated states from the second column were assigned to the experimental states from the first column (and table 1).

E_i [keV]	J_i^π	E_f [keV]	J_f^π	b^{exp} [%]	b^{SM1} [%]	b^{SM2} [%]
291	$5/2_1^+$	0	$1/2_1^+$	18	4	6
		12	$3/2_1^+$	100	100	100
303	$3/2_2^+$	0	$1/2_1^+$	100	54	83
		12	$3/2_1^+$	86	100	100
540	$1/2_2^+$	291	$5/2_1^+$	–	0	0
		0	$1/2_1^+$	–	100	100
		12	$3/2_1^+$	100	25	14
577	$7/2_1^+$	291	$5/2_1^+$	–	0	0
		302	$3/2_2^+$	–	4	4
		12	$3/2_1^+$	100	100	100
631	$5/2_2^+$	291	$5/2_1^+$	6	10	11
		302	$3/2_2^+$	–	0	0
		0	$1/2_1^+$	17	5	5
		12	$3/2_1^+$	100	100	100
676	$3/2_3^+$	291	$5/2_1^+$	5	9	8
		302	$3/2_2^+$	4	1	0
		539	$1/2_2^+$	–	0	0
		577	$7/2_1^+$	–	0	0
		0	$1/2_1^+$	29	5	4
		12	$3/2_1^+$	100	100	100
862	$3/2_4^+$	291	$5/2_1^+$	82	11	10
		302	$3/2_2^+$	9	3	5
		539	$1/2_2^+$	–	6	3
		577	$7/2_1^+$	–	0	0
		631	$5/2_2^+$	–	0	0
		0	$1/2_1^+$	–	49	54
		12	$3/2_1^+$	97	100	96
		291	$5/2_1^+$	100	71	100
858	$3/2_5^+$	302	$3/2_2^+$	70	1	26
		539	$1/2_2^+$	–	15	29
		577	$7/2_1^+$	–	0	0
		631	$5/2_2^+$	2	7	8
		676	$3/2_3^+$	–	1	2
		0	$1/2_1^+$	82	100	100
		12	$3/2_1^+$	100	40	58
		291	$5/2_1^+$	45	20	30
886	$5/2_3^+$	302	$3/2_2^+$	30	43	6
		539	$1/2_2^+$	–	41	22
		577	$7/2_1^+$	–	0	0
		631	$5/2_2^+$	2	0	0
		676	$3/2_3^+$	–	11	3
		0	$1/2_1^+$	6	4	4
291	$5/2_1^+$	12	$3/2_1^+$	10	59	57
		302	$3/2_2^+$	44	100	63
		291	$5/2_1^+$	100	62	100

Table 6. Continued.

E_i [keV]	J_i^π	E_f [keV]	J_f^π	b^{exp} [%]	b^{SM1} [%]	b^{SM2} [%]
		539	$1/2_2^+$	1	0	1
		577	$7/2_1^+$	4	0	0
		631	$5/2_2^+$	6	13	11
		676	$3/2_3^+$	1	10	9
		858	$3/2_5^+$	–	0	0
		862	$3/2_4^+$	–	0	0

Table 7. Spectroscopic factors, $(2j+1)S_{lj}$, predicted for low-lying states in ^{133}Ba by the two shell model calculations, compared to the corresponding experimental values. The calculated states from the second column were assigned to the experimental states from the first column (and table 1).

E_x [keV]	J_i^π	$(2j+1)S_{lj}^{exp}$	$(2j+1)S_{lj}^{SM1}$	$(2j+1)S_{lj}^{SM2}$
0	$1/2_1^+$	0.47	0.72	0.65
540	$1/2_2^+$	–	0.00	0.00
1248	$1/2_3^+$	0.10	0.02	0.10
12	$3/2_1^+$	1.13	0.73	0.88
303	$3/2_2^+$	0.19	0.64	0.43
676	$3/2_3^+$	0.03	0.00	0.01
862	$3/2_4^+$	–	0.03	0.01
858	$3/2_5^+$	0.24	0.07	0.16
291	$5/2_1^+$	–	0.00	0.00
630	$5/2_2^+$	0.30	0.11	0.11
886	$5/2_3^+$	0.12	0.00	0.00
577	$7/2_1^+$	0.12	0.01	0.01
288	$11/2_1^-$	2.30	2.06	2.46

the wave functions have a rather mixed character, even for the lowest states.

Table 6 shows a comparison between the experimental branching ratios of the low-lying positive-parity states and those calculated by shell model in the two schemes. Except for the second $1/2^+$ state, the first four excited $3/2^+$ states, and three $5/2^+$ states are reasonably well described, generally better for the SM2 calculation. Note that we have assigned the calculated $3/2_5^+$ state to the state at 858 keV and tentatively the calculated $3/2_4^+$ state to the state at 862 keV, which was previously assigned as a positive-parity state, and probably was weakly excited and not resolved from the 858 keV one in our experiment. These assignments are also in agreement with those suggested by the observed spectroscopic factors given in table 7. In table 7, one observes also that the predictions of the SM2 calculations are generally better and they explain reasonably well the experimental spectroscopic factors. Table 8 gives the predictions of the SM2 calculations for the electromagnetic $M1$ and $E2$ reduced transition probabilities, which are not yet measured in this nucleus.

Table 8. Reduced transition probabilities, $B(M1)$ and $B(E2)$, for transitions between low-lying states in ^{133}Ba , calculated with the SM2 effective interaction.

E_i [keV]	J_i^π	E_f [keV]	J_f^π	$B(M1)$ [W.u.]	$B(E2)$ [W.u.]
12	$3/2_1^+$	0	$1/2_1^+$	0.030	16.1
291	$5/2_1^+$	0	$1/2_1^+$	–	27.2
		12	$3/2_1^+$	0.069	35.6
303	$3/2_2^+$	0	$1/2_1^+$	0.017	23.8
		12	$3/2_1^+$	0.025	20.7
		291	$5/2_1^+$	0.225	12.4
540	$1/2_2^+$	0	$1/2_1^+$	0.006	0.0
		12	$3/2_1^+$	0.000	1.1
		291	$5/2_1^+$	–	1.9
		302	$3/2_2^+$	0.002	0.6
577	$7/2_1^+$	12	$3/2_1^+$	–	39.1
		291	$5/2_1^+$	0.016	2.5
		302	$3/2_2^+$	–	6.8
631	$5/2_2^+$	0	$1/2_1^+$	–	13.2
		12	$3/2_1^+$	0.161	5.6
		291	$5/2_1^+$	0.077	6.8
		302	$3/2_2^+$	0.000	22.5
		539	$1/2_2^+$	–	1.6
		577	$7/2_1^+$	0.054	1.0
676	$3/2_3^+$	0	$1/2_1^+$	0.000	0.4
		12	$3/2_1^+$	0.008	0.0
		291	$5/2_1^+$	0.004	0.7
		302	$3/2_2^+$	0.002	1.0
		539	$1/2_2^+$	0.026	22.7
		577	$7/2_1^+$	–	5.6
		631	$5/2_2^+$	0.019	0.0
862	$3/2_4^+$	0	$1/2_1^+$	0.001	0.1
		12	$3/2_1^+$	0.002	0.0
		291	$5/2_1^+$	0.006	0.5
		302	$3/2_2^+$	0.002	0.1
		539	$1/2_2^+$	0.008	7.8
		577	$7/2_1^+$	–	0.2
		631	$5/2_2^+$	0.007	1.7
		676	$3/2_3^+$	0.003	8.5
858	$3/2_5^+$	0	$1/2_1^+$	0.002	0.1
		12	$3/2_1^+$	0.001	0.4
		291	$5/2_1^+$	0.002	0.2
		302	$3/2_2^+$	0.000	0.0
		539	$1/2_2^+$	0.008	6.5
		577	$7/2_1^+$	–	0.2
		631	$5/2_2^+$	0.000	0.0
		676	$3/2_3^+$	0.005	8.7
886	$5/2_3^+$	0	$1/2_1^+$	–	0.2
		12	$3/2_1^+$	0.003	0.0
		291	$5/2_1^+$	0.015	0.0
		302	$3/2_2^+$	0.010	0.1
		539	$1/2_2^+$	–	3.7

Table 8. Continued.

E_i [keV]	J_i^π	E_f [keV]	J_f^π	$B(M1)$ [W.u.]	$B(E2)$ [W.u.]
		577	$7/2_1^+$	0.000	0.2
		631	$5/2_2^+$	0.021	0.0
		676	$3/2_3^+$	0.032	3.8
		858	$3/2_5^+$	0.238	0.3
		862	$3/2_4^+$	0.153	14.0

4 Summary

Excited states in the ^{133}Ba nucleus were studied with the $^{132}\text{Ba}(d, p)^{133}\text{Ba}$ reaction at 24.0 MeV, with a polarized deuteron beam and using the Q3D Munich spectrograph. These measurements allowed many unambiguous spin-parity assignments for states up to about 2.2 MeV excitation. The better knowledge of the low-energy low-spin states in this nucleus allowed a detailed comparison with different model calculations. Such calculations were first made with the Interacting Boson-Fermion model. Although the core nucleus ^{134}Ba approximates well the critical-point symmetry $E(5)$, different supersymmetric schemes proposed for odd-mass nuclei do not fit the experimental properties of ^{133}Ba . The best agreement for the positive-parity states was obtained when all four active positive-parity orbitals are coupled to the IBA ^{134}Ba core. Still, the observed fragmentation of the four orbitals, as observed in this (d, p) reaction study, is not satisfactorily explained. Calculations were made also with the spherical-shell model with an effective interaction determined from the realistic NN potential CD-Bonn-2000. The configuration space used for diagonalization included all single-particle orbitals in the $Z, N = 50\text{--}82$ shells and it was truncated such that only one or two neutron holes were allowed in the $g_{7/2}$ and $d_{5/2}$ orbitals, respectively, and not more than four or two protons were allowed to be excited from the lowest orbital $g_{7/2}$ into the $d_{5/2}$ orbital or into the higher ones ($d_{3/2}$, $s_{1/2}$, and $h_{11/2}$), respectively.

These calculations describe reasonably well the known properties (branching ratios and spectroscopic factors) of the low-lying low-spin positive-parity states, and provide predictions for the electromagnetic decay transition probabilities, which are practically missing in this nucleus. The only measured value is that of the transition of 12 keV from the $3/2_1^+$ state to the $1/2_{gs}^+$, which is $B(M1) = 0.024(1)$ W.u. [8], in agreement with the predicted value of 0.030 W.u. Electromagnetic decay probability measurements in ^{133}Ba are highly desirable in order to better assess the quality of the predictions of different model calculations.

We thank the accelerator staff at the Maier-Leibnitz Laboratory for the excellent conditions during the experiments, and A. Moro for his help on the CDCC method and the FRESKO code. We acknowledge support from the Deutsche Forschungsgemeinschaft under the grant 436 RUM 17/1/07. This work

was partly funded by the Romanian National Authority for Scientific Research under the PNCDI2 programme, contract No. ID-117/01.10.2007.

References

1. F. Iachello, A. Arima, *The Interacting Boson Model* (Cambridge University Press, Cambridge, 1987).
2. R.F. Casten, P. von Brentano, Phys. Lett. **152**, 22 (1985).
3. R.F. Casten, N.V. Zamfir, Phys. Rev. Lett. **85**, 3584 (2000).
4. F. Iachello, Phys. Rev. Lett. **85**, 3580 (2000).
5. F. Iachello, Phys. Rev. Lett. **95**, 052503 (2005).
6. C.E. Alonso, J.M. Arias, A. Vitturi, Phys. Rev. Lett. **98**, 052501 (2007); Phys. Rev. C **75**, 064316 (2007).
7. M.S. Fetea, R.B. Cakirli, R.F. Casten, D.D. Warner, E.A. McCutchan, D.A. Meyer, A. Heinz, H. Ai, G. Gürdal, J. Qain, R. Winkler, Phys. Rev. C **73**, 051301(R) (2006).
8. S. Rab, Nucl. Data Sheets **75**, 491 (1995); the ENSDF database, evaluated and maintained at the Brookhaven National Laboratories, <http://www.nndc.bnl.gov>.
9. E.A. Henry, R.A. Meyer, Phys. Rev. C **13**, 2501 (1976).
10. K. Miyano, Y. Kato, J. Phys. Soc. Jpn. **49**, 444 (1980).
11. D. von Ehrenstein, G.C. Morrison, J.A. Nolen jr., N. Williams, Phys. Rev. C **1**, 2066 (1970).
12. J. Gizon, A. Gizon, D.J. Horen, Nucl. Phys. A **252**, 509 (1975).
13. R. Hertenberger, A. Metz, Y. Eisermann, K. Elabiary, A. Ludewig, C. Pertl, S. Trieb, H.-F. Wirth, P. Schiemenz, G. Graw, Nucl. Instrum. Methods A **536**, 266 (2005).
14. N. Chauvin *et al.*, Nucl. Instrum. Methods A **521**, 149 (2004).
15. M. Löffler, H.J. Scheerer, H. Vonach, Nucl. Instrum. Methods **111**, 1 (1973).
16. H.-F. Wirth, H. Angerer, T. von Egidy, Y. Eisermann, G. Graw, R. Hertenberger, Beschleunigerlaboratorium München Annual Report, 2000, p. 71.
17. H.-F. Wirth, PhD Thesis, Technische Universität München, 2001 (<http://tumb1.biblio.tu-muenchen.de/publ/diss/ph/2001/wirth.html>).
18. P.R. Christensen, B. Herskind, R.R. Borchers, L. Westgaard, Nucl. Phys. A **102**, 481 (1967); W. Booth, S. Wilson, Nucl. Phys. A **247**, 126 (1975).
19. G. Suliman, D. Bucurescu, R. Hertenberger, H.-F. Wirth, T. Faestermann, R. Krücken, T. Behrens, V. Bildstein, K. Eppinger, C. Hinke, M. Mahgoub, P. Meierbeck, M. Reithner, S. Schwertel, N. Chauvin, Eur. Phys. J. A **36**, 243 (2007).
20. P.D. Kunz, Computer code CHUCK3, University of Colorado, unpublished.
21. RIPL-2, Reference Input Parameter Library, <http://www-nds.iaea.org/RIPL-2>.
22. J.M. Lohr, W. Haerberli, Nucl. Phys. A **232**, 381 (1974) (RIPL ref. 6100).
23. F.D. Becchetti jr., G.W. Greenlees, Phys. Rev. **182**, 1190 (1969) (RIPL ref. 4101).
24. C.M. Perey, F.G. Perey, Phys. Rev. **132**, 755 (1963) (RIPL ref. 6101).
25. J. Bojowald *et al.*, Phys. Rev. C **38**, 1153 (1988) (RIPL ref. 6400).
26. A.J. Koning, J.P. Delaroche, Nucl. Phys. A **713**, 231 (2003) (RIPL ref. 5405).

27. N. Keeley, N. Alamanos, V. Lapoux, Phys. Rev. C **69**, 064604 (2004).
28. M. Kawai, Prog. Theor. Phys. Suppl. **89**, 11 (1986); Y. Iseri, M. Yahiro, M. Kamimura, Prog. Theor. Phys. Suppl. **89**, 32 (1986).
29. N. Austern, Y. Iseri, M. Kamimura, M. Kawai, G. Rauscher, M. Yahiro, Phys. Rep. **154**, 125 (1987).
30. I.J. Thompson, Comput. Phys. Rep. **7**, 167 (1988).
31. F. Iachello, O. Scholten, Phys. Rev. Lett. **43**, 679 (1979).
32. O. Scholten, Computer codes PHINT and FBEM, KVI Internal Report No. 63, 1979.
33. O. Scholten, Computer codes ODDA and PBEM, KVI Internal Report No. 252, 1982.
34. C.E. Alonso, J.M. Arias, L. Fortunato, A. Vitturi, Phys. Rev. C **72**, 061302(R) (2005).
35. R. Bijker, A.E.L. Dieperink, Nucl. Phys. A **379**, 221 (1982).
36. B.S. Reehal, R.A. Sorensen, Phys. Rev. C **2**, 819 (1970).
37. S. Pascu, private communication; in preparation.
38. D. Bucurescu, T. von Egidy, H.-F. Wirth, N. Mărginean, U. Köster, W. Schauer, I. Tomandl, G. Graw, A. Metz, R. Hertenberger, Y. Eisermann, Nucl. Phys. A **672**, 21 (2000).
39. NuShellX code - W.D.M. Rae, Knoll House, Garsington, Oxford, <http://knollhouse.org>.
40. C. Machleid, Phys. Rev. C **63**, 024001 (2001).
41. M. Hjorth-Jensen *et al.*, Phys. Rep. **261**, 125 (1995); M. Hjorth-Jensen, *et al.*, J. Phys. G **22**, 321 (1996); T. Engeland, M. Hjorth-Jensen, G.R. Jansen, *CENS, a Computational Environment for Nuclear Structure*, in preparation.